



## Commercial brucite, a worldwide used raw material deemed safe, can be contaminated by asbestos

Daniele Malferrari<sup>1</sup>, Dario Di Giuseppe<sup>1,2,\*</sup>, Valentina Scognamiglio<sup>1</sup>,  
Alessandro F. Gualtieri<sup>1</sup>

<sup>1</sup> Department of Chemical and Geological Sciences, University of Modena and Reggio Emilia, Modena, Italy

<sup>2</sup> Department of Sciences and Methods for Engineering, University of Modena and Reggio Emilia, Modena, Italy

### ARTICLE INFO

Submitted: March 2021

Accepted: April 2021

Available on line: July 2021

\* Corresponding author:  
ddigiuse@unimore.it

Doi: 10.13133/2239-1002/17384

How to cite this article:  
Malferrari D. et al. (2021)  
Period. Mineral. 90, 317-324

### ABSTRACT

Brucite is a raw material used in several applications and worldwide traded. The main active deposits are located in North America, North Europe and China and the extracted material is worked and delivered all over the world without any particular precaution as it is considered a safe inert product. But is it really true? Applying a consolidated protocol of analysis for the detection and characterization of fibers, we found asbestos in a sample of commercial brucite. The analyzed material is primarily composed of plate-like crystals of brucite; nevertheless, chemical and mineralogical analyses revealed the presence of serpentine, while morphometric observation through electron microscopy confirmed the occurrence of respirable regulated chrysotile (serpentine asbestos) fibers. The individual fibers making up the chrysotile bundles have length  $>5 \mu\text{m}$ , width  $<3 \mu\text{m}$ , length/width ratio  $>3$ , and their concentration in the investigated product is 169 mg/kg (0.02 wt%). Although paragenesis of brucite with chrysotile has been known for a long time, never before was documented a commercial brucite, distributed worldwide, contaminated with asbestos. In the light of these results, we think that certification of the absence of asbestos should be imposed to the brucite mining companies and distributors; otherwise, users should always include a careful inspection on incoming materials, at least by electron microscopy, to rule out the occurrence of asbestos.

Keywords: Asbestos, brucite; chrysotile; raw materials; respirable fibers; serpentine.

### INTRODUCTION

Brucite  $[\text{Mg}(\text{OH})_2]$  is a high market-growth potential raw material mainly occurring in ultramafic deposits as an alteration product (serpentinization) of dunites and peridotites, or in Mg-rich carbonate-hosted deposits affected by high-temperature and low-pressure metamorphism (Simandl et al., 2007; Manuella, 2011; Deer et al., 2013; Guan et al., 2014). Given the frequent concomitant occurrence of fibrous minerals in the former (Davis et al., 1985; Guthrie, 1992; Gualtieri et al., 2014; Pollastri et al., 2016), the latter, like those in Quebec (Keith, 1946; Simandl et al., 2007), Norway (Øvereng,

2000), Nevada (Schilling, 1968), and Texas (Newman and Hoffman, 1996), are preferred as exploitable sources of the mineral.

Brucite crystallizes forming massive cryptocrystalline aggregates, pseudo-hexagonal plates and elongated fibrous crystals; the latter variety, common in ultramafic rock, is also known as *nemalite*. In the recent past, the existence of the fibrous form of brucite had raised doubts about the safety of this material (Pott et al., 1974; Kaw et al., 1982); however, most of the studies that described nemalite as a potentially hazardous material were after discredited, as it was found that samples used in the clinic-tests came

from ultramafic rocks and were polluted up to 10 wt% by respirable chrysotile fibers (Davis et al., 1985; Guthrie, 1992). Nevertheless, the possible occurrence of asbestos minerals together with brucite should arise concern. Even if carbonate-hosted deposits of brucite are deemed safe, it should be considered that the presence of a small amount of silica in the protolith may result in the recrystallization of (fibrous) silicates in paragenesis with brucite (Simandl et al., 2007). Notwithstanding this, commercial brucite is considered a safe material that can be handled without any proper protective devices. It is widely used in several applications such as flame retardant and smoke suppression for insulating materials and coatings (Barik and Badamali et al., 2017), as an inorganic additive in ceramic inks and pigments (Auxilio et al., 2010; Chen et al., 2018), for CO<sub>2</sub> sequestration (Assima et al., 2013; Harrison et al., 2013; Lechat et al., 2016; Rausis et al., 2020), in cement-based composites (Guan et al., 2014; Xiong et al., 2015; Sheng et al., 2019; Yuanyi et al., 2019), and as MgO source (Liu et al., 2018).

Although most occupational health problems arise from processing fibrous minerals, health damages may also occur from managing raw materials naturally contaminated with asbestos (IARC, 2012; Gualtieri et al., 2018; Fitzgerald et al., 2019). Noteworthy in this regard are the health problems experienced by the employees of the vermiculite plant in Libby, Montana, U.S.A. (Horton et al., 2008; Larson et al., 2010) where, between 1924 and 1990, were extracted and processed about 5.8 Mt of raw vermiculite containing amphibole fibers. A retrospective cohort study of workers exposed to Libby's vermiculite found an excess of deaths from lung cancer and asbestosis of 20 and 40 %, respectively, compared to the mean mortality in Montana and the United States (Ward et al., 2012).

In this context, in recent past, remarkable activities were promoted to discover traces of asbestos in several raw materials considered hazardous-free such as, for example, talc and feldspar (Gualtieri et al., 2018; Fitzgerald et al., 2019; Dyer, 2019; Tran et al., 2019). In light of the results obtained from these researches, some districts (e.g., Emilia Romagna region, Italy) made mandatory specific tests for raw materials already known to be potentially (naturally) contaminated by respirable regulated fibers. In contrast, processing and worldwide brucite trade, which produce easily inhalable volatile dusts, are not subject to any restriction as brucite is assumed to be a safe raw material. Therefore, our intent is to warn both the scientific community and the international market that brucite may present risks, particularly when it is imported from countries that allow the "safe use" of chrysotile asbestos (Frank and Joshi, 2014; IBAS, 2020).

## MATERIAL AND METHODS

### Material

The analyzed sample is a commercial brucite used, for example, by several companies in northern Italy for the production of traditional ceramics (stoneware tile) and manufacture of glass. The presence of chrysotile asbestos has not been reported nor certified as its use is permitted in the country from which it was imported (Frank and Joshi, 2014; IBAS, 2020). A preliminary characterization of a representative sample was carried out by a private laboratory that unambiguously identified the occurrence of asbestos fibers. The same representative sample was recently delivered to our academic lab for a full chemical and mineralogical characterization aimed at confirming the presence, nature and amount of asbestos minerals. Contamination did not occur during material processing as fibers were also found in a sample of the same product composed of centimeter thick fragments. Therefore, as pointed out above, it is the close mineralogical relationship between brucite and chrysotile that led to the co-mineralization.

### Methods and preparation of sample

We considered a set of measures based on morphometric, mineralogical and chemical analyses for fibers detection and characterization (Gualtieri et al., 2018; Di Giuseppe et al., 2019; Zoboli et al., 2019). The analytical protocol encompassing the use of transmission electron microscopy and polarized light microscopy, usually applied to fibers detection, was not considered here as the occurrence of respirable chrysotile fibers was already clearly highlighted by scanning electron microscopy.

The detailed observation of the sample was performed using a Scanning Electron Microscope (SEM), JSM-6010PLUS/LA (JEOL, Hillsboro, OR, USA) equipped with an Energy Dispersive X-ray (EDX) spectrometer. For the SEM quantitative analysis, the procedure suggested by the Italian Minister Decree 06.09.94 was applied (Italian Ministry of Health, 1994; Gualtieri et al., 2018). An amount of 5 mg of the sample was suspended in 200 ml of deionized water with 0.1 vol% surfactant additive (dioctylsodium sulfocinate, C<sub>20</sub>H<sub>37</sub>NaO<sub>7</sub>S, CAS no. 577-11-7), and ultrasonicated for 10 min to prompt the separation of the particles. A volume of 6 ml of this suspension was collected at different levels in a becker and put into a filtering system, allowing random deposition of the particles on polycarbonate filters (20 mm<sup>2</sup> surface, 0.45 μm porosity). The filter was dried at 55 °C and weighed. The final weight of the material deposited on the filter was 0.1 mg. The filter was mounted on an aluminum stub and gold-coated (10 nm of thickness). Images were acquired using secondary electrons. A surface of 1 mm<sup>2</sup> of the filter was investigated, working at 4000× for a total of

130 analysis fields. The concentration  $C$  of the chrysotile fibers was calculated using the equation below:

$$C = \frac{A \cdot (w_a)}{n \cdot a \cdot W} \cdot 10^6 \quad (1)$$

with  $A$ =filter surface ( $\text{mm}^2$ );  $w_a$ =total weight of counted fibers (mg) using a density for chrysotile of  $2.53 \text{ g/cm}^3$ ;  $n$ =number of analyzed fields;  $a$ =area of the fields ( $\text{mm}^2$ );  $W$ =weight of the sample on the filter (mg).

X-ray powder diffraction (XRPD) pattern was recorded from a randomly oriented powdered sample obtained after the quartering procedure. Measurement was carried out at room temperature using an X'Pert PRO diffractometer (Philips, Almelo, The Netherlands) equipped with first generation Real Time Multiple Strip (RTMS) detector. Experimental conditions were: incident beam,  $\text{Cu K}\alpha$  radiation at 40 kV and 40 mA; filter, nickel; Soller slits, 0.04 rad; anti-scatter mask, 20 mm; anti-scatter slit,  $1/4^\circ$ ; divergence slit,  $1/4^\circ$ . Diffracted beam: anti-scatter mask, 5.0 mm; Soller slits, 0.04 rad; step size of  $0.0170^\circ 2\theta$  per s. The diffraction pattern was recorded in the  $3\text{--}75^\circ 2\theta$  range after calibrating the diffractometer with NIST SRM 676a (alumina powder, corundum structure).

The thermogravimetric (TGA) and thermodifferential (DTA) analyses were carried out with a Seiko SSC 5200 thermal analyzer (Seiko, Chiba, Japan) coupled with a quadrupole mass spectrometer GeneSys Quadstar 422 (ESS Ltd. Cheshire, UK) to simultaneously detect the

gasses evolved during thermal reactions (MSEGA). Gas sampling by the spectrometer was through an inert, fused silicon capillary heated to prevent gas condensing. Experimental conditions were: heating rate:  $20^\circ \text{C}/\text{min}$ ; heating range:  $25\text{--}1150^\circ \text{C}$ ; data measurement: every 0.5 s; DTA reference:  $\alpha$ -alumina powder; purging gas: ultrapure helium, flow rate:  $100 \mu\text{L}/\text{min}$ . Mass analyses were carried out in multiple ion detection mode measuring the  $m/z$  ratios (i.e., the dimensionless ratio between the mass number  $m$  and the charge  $z$  of an ion) 18, 30, 44, 64 to detect the emission of  $\text{H}_2\text{O}$ ,  $\text{NO}$ ,  $\text{CO}_2$ , and  $\text{SO}_2$ , respectively; a secondary electron multiplier detector set at 900 V was employed with 1 s of integration time on each measured mass.

Major element determination was achieved through a wavelength dispersive PW 1480 X-ray fluorescence (XRF) spectrometer (Philips, Almelo, Netherlands) on powder pressed pellets. When the concentration of an element measured in XRF was found to be less than 0.1 wt%, it was refined on acid digested sample through Inductively Coupled Plasma Optical Emission Spectroscopy (ICP-OES) Perkin Elmer Optima 4200 DV (Perkin Elmer, Waltham, Massachusetts, U.S.A.) calibrated with certified standard solutions.

## RESULTS

Scanning electron microscopy images (Figure 1) show that brucite primarily forms aggregates of plate-like crystals (Figures 1 a b), whereas crystals with an elongated

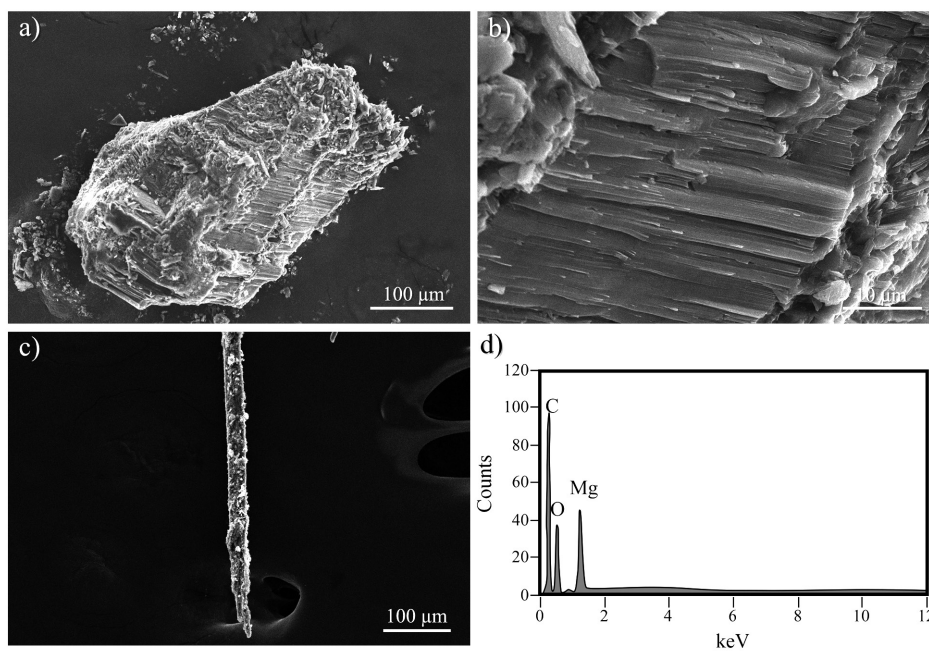


Figure 1. SEM images and EDX spectrum. Brucite appears as a conglomerate of platy (a, b) and elongated (c) crystals; d) representative EDX spectrum of the sample in Figure 1c.

morphology (Figures 1c) were occasionally observed. A representative EDX spectrum of brucite is shown in Figure 1d. Figure 2 shows particles in which long bundles of mineral fibers occur (Figure 2 a-c). The EDX spectrum recorded onto the fibers (Figure 2d) revealed an elemental composition (Si and Mg) compatible with chrysotile. The individual fibers making up the chrysotile bundles have length  $>5 \mu\text{m}$ , width  $<3 \mu\text{m}$ , length/width ratio  $>3$  (Figure 2), and meet the criteria for a respirable (regulated) fiber according to the World Health Organization directives (WHO, 1997). The mean concentration of regulated chrysotile fibers in the investigated product is 169 mg/kg (0.02 wt%) as calculated using Equation (1). Additionally, SEM revealed the occurrence of lizardite (Supplementary Figure S1), muscovite/phlogopite (Supplementary Figure S2), phlogopite (Supplementary Figure S3), magnetite (Supplementary Figure S4), and fragments of Si-, Al- and Ca-bearing phase(s) (Supplementary Figure S5).

X-ray powder diffraction pattern (Figure 3) indicates that, in addition to brucite, also occur serpentine (chrysotile and lizardite, as better highlighted by SEM), calcite ( $\text{CaCO}_3$ ), magnesite ( $\text{MgCO}_3$ ) and, to a lesser extent, dolomite; these results are confirmed by chemical measurements that show significant amounts of Si and Ca together with Mg which, of course, is the most abundant element (Table 1).

The thermogravimetric (TGA) and its first derivative (DTG) curves (Figure 4a) show five main thermal events: (1) 122-158 °C (maximum reaction rate at 137 °C, mass loss of 0.096 wt%); (2) 329-511 °C (457 °C, 23.95 wt%); (3) 512-613 °C (575 °C, 1.84 wt%); (4) 614-801 °C (717 °C, 4.50 wt%); (5) a tail well evident in the previous reaction at about 656 °C. The thermodifferential analyses (DTA, Figure 4a) shows a further exothermic reaction (6), with a maximum at about 870 °C, which does not involve any mass change. Reaction (1), together with the slight mass variation that occurs in the thermal range between 25 and 122 °C, is due to the release of more or less strongly adsorbed water molecules on the mineral surface, as also confirmed by MSEGAs curves (Figure 4b,  $m/z=18$ ). Reaction (2) is mainly due to the dehydroxylation of brucite (Kissinger, 1957), as evidenced by the water release. Almost simultaneously, however, the release of  $\text{CO}_2$  (Figure 4b,  $m/z=44$ ) also occurs following a first decarbonation of the dolomite (Mackenzie, 1970; Taufiq-Yap et al., 2014; Bloise et al., 2016) according to the known reaction  $\text{CaMg}(\text{CO}_3)_2 \rightarrow \text{MgO} + \text{CaCO}_3$ . Reaction (3) is exclusively associated with the release of  $\text{CO}_2$  and it is attributable to the decarbonation of magnesite (Mackenzie, 1970). Reactions (4) and (5), almost completely superimposed, involve the release of water (dehydroxylation of the serpentine) and

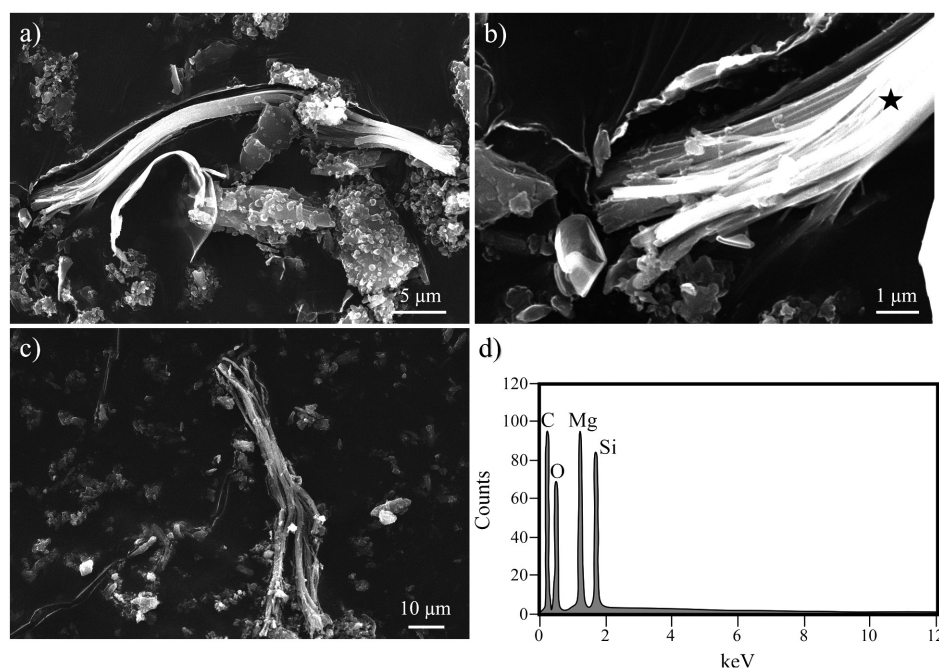


Figure 2. SEM images and EDX spectrum. a) Bundle of chrysotile fibers with an average length and width of 42 and 0.2  $\mu\text{m}$ , respectively, b) magnification of Figure 2a, c) Chrysotile forms bundles composed of many curvilinear fibers, which tend to divide along the elongation axis; fibers have an average length and width of 75  $\mu\text{m}$  and 0.5  $\mu\text{m}$ , respectively, d) EDX spectrum of the chrysotile bundles highlighted with a black star in Figure 2b.

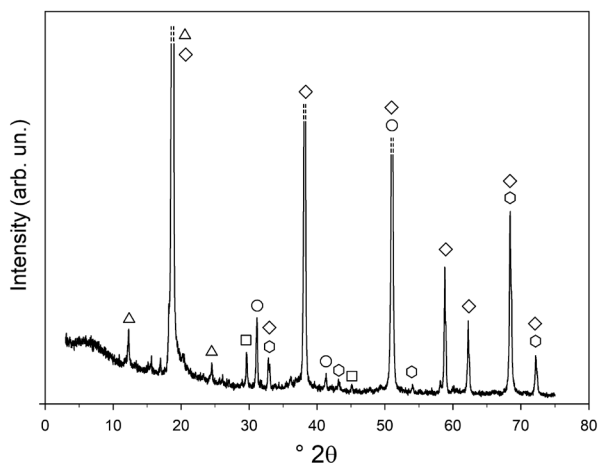


Figure 3. XRPD pattern of the brucite sample. Labels: triangles (serpentine), diamonds (brucite), squares (calcite), circles (dolomite) and hexagon (magnesite).

CO<sub>2</sub> (decarbonation of calcite, both pristine and that derived from the partial thermal decomposition of the dolomite). Reaction (6) in the DTA curve is due to the recrystallization of the serpentine in forsterite occurring after dihydroxylation (Korami, 1984; Cattaneo et al., 2003; Bloise et al., 2016). In the considered thermal range do not occur reactions that involve the release of NO ( $m/z=30$ ) and SO<sub>2</sub> ( $m/z=64$ ).

## DISCUSSION

To date, the presence of asbestos in worldwide traded commercial brucite had never been reported, hence this product was assumed to be safe; on the contrary, this research, by applying a complete chemical and mineralogical characterization, has shown that this view must be reconsidered.

By combining the results of chemical and TGA-MSEGA measurements it is possible to estimate brucite and serpentine content. However, to gain this goal, it is necessary to: i) consider an ideal serpentine without isomorphic substitutions; ii) omit the occurrence of other silicates (i.e., those found in trace through SEM-EDX, Supplementary Figures S1-S3, S5) and of Si bearing amorphous phases; iii) attribute the thermal

reaction (2) entirely to brucite (really, as indicated by the MSEGA measurements, also decarbonation of dolomite contributes a little to the overall mass loss). Once fixed these constraints, the maximum amounts of serpentine and brucite are 4.7 and 77.5 wt% respectively. Although SEM observations and calculations (Equation 1) suggested that the amount of regulated chrysotile fibers is considerably lower than 4.7 wt%, it should be remembered that many countries (Italy is included) do not allow the occurrence (also minimal) of respirable fibers in raw materials.

The high quality and safety of raw materials is a prerequisite for any industrial or manufacturing sector. However, considering the precautionary principle and good practices regarding safety in the workplace, all raw materials that come into contact with workers must be tested for toxic/hazardous contaminants, especially when they may be “well hidden” within a material unanimously considered safe. On the other hand, it is also true that the quality certificates provided by raw material suppliers are usually satisfactory, and companies are improbable to invest considerable effort in expansive and non-statutory analyses. Nevertheless, concerning brucite, it would be sufficient to check the chemical composition carefully (usually indicated on the safety data sheet) and, once verified the presence of a significant amount of silicon, to carry out further investigations (e.g., XRPD and SEM-EDX which are fairly common techniques). Specifically, this means that commercial brucite samples from all over the world should be checked for the presence of asbestos to avoid situations similar to those of commercial talc and feldspar (several litigations are in progress, especially in the United States). Without these safety checks, it is possible that brucite products containing asbestos fibers freely circulate in the world market, are used, worked (e.g., grinded) thus exposing to asbestos both the work force in the manufacture site and the population getting in contact with the final products.

Nevertheless, several general questions remain open. First, the problem of asbestos in a global world. Based on numerous scientific evidences, asbestos minerals are included by the International Agency for Research on Cancer in the *Group 1* “substance carcinogenic to humans” (IARC, 2012). Nowadays, a worldwide ban exists for amphibole asbestos (except Bolivia and India); in contrast,

Table 1. Major elements chemical analyses (oxide wt%). Values are the mean of three replicates, standard deviation is shown in parentheses. LOI: Loss on ignition at 1000°C.

	SiO <sub>2</sub>	TiO <sub>2</sub>	Al <sub>2</sub> O <sub>3</sub>	Fe <sub>2</sub> O <sub>3</sub>	MnO	MgO	CaO	Na <sub>2</sub> O	K <sub>2</sub> O	P <sub>2</sub> O <sub>5</sub>	LOI
Brucite	2.04	0.014	0.24	0.31	0.032	64.33	1.91	0.031	0.093	0.040	30.96
	(0.11)	(0.005)	(0.04)	(0.06)	(0.007)	(0.91)	(0.11)	(0.009)	(0.007)	(0.010)	(1.01)

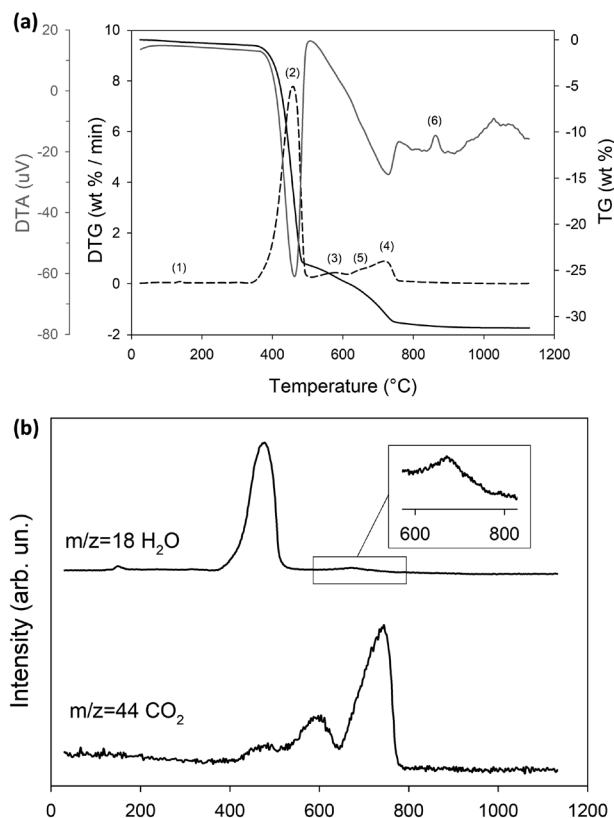


Figure 4. Thermal behavior of the brucite sample. a) TG (solid black line), DTG (dashed black line) and DTA (solid gray line). b) MSEG curves. Maxima on the DTG/DTA curve denote exothermic reactions. Numbers on the DTG/DTA curves refer to reactions described in the text.

the trade and use of chrysotile is still allowed in several Nations (Di Giuseppe et al., 2021; IBAS, 2020; Ilgren et al., 2015) despite the global ban invoked by the World Health Organization and supported by the International Labour Organization. However, the real problem is that the countries that deny the toxicity of chrysotile (Camus, 2001; Bernstein et al., 2013), extract and distribute it all over the world without precautions, with the complicity of globalization and the “no labelling” imposed by the Rotterdam Convention (IBAS, 2019).

In turn, this matter raises the issue of the free circulation of natural raw materials which may contain asbestos in the world market, especially in those countries that have banned also chrysotile. This problem widens significantly if are also considered other raw materials with composition and genesis compatible with that of asbestos minerals like, for example, diopside ( $\text{CaMgSi}_2\text{O}_6$ ) which, likewise, should be carefully checked to exclude the contamination with asbestos; otherwise, the discovery could be done too late when the raw material is used in the production steps.

## CONCLUSIONS

This research aims to warn both the scientific community and the international market that trade, manage and use commercial brucite that it may be contaminated by asbestos. By applying a multi-analytic protocol based on morphometric, mineralogical and chemical analyses, respirable chrysotile fibres were found in a commercial brucite regularly traded from a country where the use of chrysotile asbestos is allowed.

In the light of these results, we think that certification of the absence of asbestos should be imposed to the brucite mining companies and distributors; otherwise, users should always include a careful inspection, at least by electron microscopy, to rule out the occurrence of asbestos. Neglecting this hazard may results in possible contamination and impairment of the manufacture site, mainly if it includes a grinding process of the raw material. Although the primary goal is to safeguard the health of workers and end-users of a product, it is also worth remembering that these events might cost the responsible companies several billion dollars. Very recent is the case of the cosmetic talc contaminated with asbestos which, in the US, forced a cosmetic company to pay a billionaire compensation for the permanent health damages and the death of victims exposed to this product in the past. Unfortunately, the issue could be even more severe for countries with inadequate, or even absent, health surveillance protocols.

Finally, we encourage future studies to determine the occurrence of fibers able to generate airborne asbestos in other “doubtful” materials like, for example, diopside.

## ACKNOWLEDGEMENTS

We warmly acknowledge the two reviewers for their advices to improve the manuscript. This research was conducted under the project “Fibres, A Multidisciplinary Mineralogical, Crystal-Chemical and Biological Project to Amend the Paradigm of Toxicity and Cancerogenicity of Mineral Fibres” (PRIN: Progetti di Ricerca di Rilevante Interesse Nazionale - grant number PRIN20173X8WA4). The study was further supported in part by the project “CCIAARE - Attuazione di un progetto di accompagnamento delle imprese nell’ambito del progetto PID impresa 4.0” financed by the Camera di Commercio di Reggio Emilia (Italy). This work does not require any Institution and Ethics approval neither informed consent and the authors declare no conflicts of interest.

## REFERENCES

- Assima G.P., Larachi F., Molson J., Beaudoin G., 2013. Accurate and direct quantification of native brucite in serpentine ores - new methodology and implications for  $\text{CO}_2$  sequestration by mining residues. *Thermochimica Acta* 566, 281-291.
- Auxilio A.R., Andrews P.C., Junk P.C., Spiccia L., 2010.

- Adsorption of ink-jet inks and anionic dyes onto Mg-Al-NO<sub>3</sub> layered double hydroxides of variable Mg: Al molar ratio. *Australian Journal of Chemistry* 63, 83-91.
- Barik S. and Badamali S.K., 2017. Layer Double Hydroxide Reinforced Polymer Bionanocomposites for Packaging Applications. In: *Bionanocomposites for Packaging Applications*. (Eds.): M. Jawaid and S. Swain, Springer Cham (Switzerland), 269-290.
- Bernstein D., Dunnigan J., Hesterberg T., Brown R., Velasco J.A.L., Barrera R., Hoskins J., Gibbs A., 2013. Health risk of chrysotile revisited. *Critical Reviews in Toxicology* 43, 154-183.
- Bloise A., Catalano M., Barrese E., Gualtieri A.F., Bursi Gandolfi N., Capella S., Belluso E., 2016. TG/DSC study of the thermal behaviour of hazardous mineral fibres. *Journal of Thermal Analysis and Calorimetry* 123, 2225-2239.
- Camus M., 2001. A ban on asbestos must be based on a comparative risk assessment. *CMAJ* 164, 491-494.
- Cattaneo A., Gualtieri A.F., Artioli G., 2003. Kinetic study of the dehydroxylation of chrysotile asbestos with temperature by in situ XRPD. *Physics and Chemistry of Minerals* 230, 177-83.
- Chen W., Liang Y., Hou X., Zhang J., Ding H., Sun S., Cao H., 2018. Mechanical grinding preparation and characterization of TiO<sub>2</sub>-coated wollastonite composite pigments. *Materials* 11, 593.
- Davis J.M., Addison J., Bolton R.E., Donaldson K., Jones A.D., Miller B.G., 1985. Inhalation studies on the effects of tremolite and brucite dust in rats. *Carcinogenesis* 6, 667-74.
- Deer W.A., Howie R.A., Zussman J., 2013. *An Introduction to the Rock-Forming Minerals*. Mineralogical Society of Great Britain and Ireland, London, UK, 498 pp.
- Di Giuseppe D., Harper M., Bailey M., Erskine B., Della Ventura G., Ardith M., Pasquali L., Tomaino G., Ray R., Mason H., Dyar M.D., Hanuskova M., Giacobbe C., Zoboli A., Gualtieri A.F., 2019. Characterization and assessment of the potential toxicity/pathogenicity of fibrous glaucophane. *Environmental Research* 178, 108723.
- Di Giuseppe D., Zoboli A., Nodari L., Pasquali L., Sala O., Ballirano P., Malferrari D., Raneri S., Hanuskova M., Gualtieri A.F., 2021. Characterization and assessment of the potential toxicity/pathogenicity of Russian commercial chrysotile. *American Mineralogist*, doi: 10.2138/am-2021-7710.
- Dyer O., 2019. Johnson & Johnson recalls its Baby Powder after FDA finds asbestos in sample. *BMJ* 367, l6118.
- Fitzgerald S., Harty E., Joshi T.K., Frank A.L., 2019. Asbestos in commercial Indian talc. *American Journal of Industrial Medicine* 62, 385-392.
- Frank A.L. and Joshi T.K., 2014. The global spread of asbestos. *Annals of Global Health* 80, 257-262.
- Gualtieri A.F., Gandolfi N.B., Pollastri S., Rinaldi R., Sala O., Martinelli G., Bacci T., Paoli F., Viani A., Vigliaturo R., 2018. Assessment of the potential hazard represented by natural raw materials containing mineral fibres - The case of the feldspar from Orani, Sardinia (Italy). *Journal of Hazardous Materials* 350, 76-87.
- Gualtieri A.F., Pollastri S., Bursi Gandolfi N., Ronchetti F., Albonico C., Cavallo A., Zanetti G., Marini P., Sala O., 2014. Determination of the concentration of asbestos minerals in highly contaminated mine tailings: An example from abandoned mine waste of Crêtaz and Èmarese (Valle d'Aosta, Italy). *American Mineralogist* 99, 1233-1247.
- Guan B., Xiong R., He R., Chen S., Ding D., 2014. Investigation of usability of brucite fiber in asphalt mixture. *International Journal of Pavement Research and Technology* 7, 193-202.
- Guthrie G.D., 1992. Biological effects of inhaled minerals. *American Mineralogist* 77, 225-243.
- Harrison A.L., Power I.M., Dipple G.M., 2013. Accelerated carbonation of brucite in mine tailings for carbon sequestration. *Environmental Science & Technology* 47, 126-134.
- Horton D.K., Bove F., Kapil V., 2008. Select mortality and cancer incidence among residents in various US communities that received asbestos-contaminated vermiculite ore from Libby, Montana. *Inhalation Toxicology* 20, 767-775.
- IARC, 2012. Asbestos (chrysotile, amosite, crocidolite, tremolite, actinolite, and anthophyllite). *IARC Monographs on the Evaluation of Carcinogenic Risks to Humans* 100C, 219-309.
- IBAS, 2019. International Ban Asbestos Secretariat. The Rotterdam Convention 2019. <http://www.ibasecretariat.org/og-lka-the-rotterdam-convention-2019.php> (accessed 2021 Feb 10).
- IBAS, 2020. International Ban Asbestos Secretariat. Current Asbestos Bans. [http://www.ibasecretariat.org/alpha\\_ban\\_list.php](http://www.ibasecretariat.org/alpha_ban_list.php) (accessed 2021 Feb 10).
- Ilgren E.B., Van Orden D.R., Lee R.J., Kamiya Y.M., Hoskins J.A., 2015. Further Studies of Bolivian Crocidolite -Part IV: Fibre Width, Fibre Drift and their relation to Mesothelioma Induction: Preliminary Findings. *Epidemiol Biostat Public Health* 12, 1-11.
- Italian Ministry of Health, 1994. Normative e metodologie tecniche di applicazione dell'art.6, comma 3, e dell'art.12, comma 2, della legge 27 marzo 1992, n.257, relativa alla cessazione dell'impiego dell'amianto. <https://www.gazzettaufficiale.it/eli/id/1994/09/20/094A5917/sg> (accessed 2021 Feb 10).
- Kaw J.L., Tilkes F., Beck E.G., 1982. Reaction of cells cultured in vitro to different asbestos dusts of equal surface area but different fibre length. *British Journal of Experimental Pathology* 63, 109-115.
- Keith M.L., 1946. Brucite deposits in the Rutherglen district, Ontario. *Geological Society of America Bulletin* 57, 967-984.
- Kissinger H.E., 1957. Reaction kinetics in differential thermal analysis. *Analytical Chemistry* 29, 1702-1706.
- Korami J., Choquette D., Kimmerle F.M., 1984. Interpretation of EGA and DTG analyses of chrysotile asbestos. *Thermochemica Acta* 76, 87-96.

- Larson T.C., Antao V.C., Bove F., 2010. Vermiculite worker mortality: estimated effects of occupational exposure to Libby amphibole. *Journal of Occupational and Environmental Medicine* 52, 555-560.
- Lechat K., Lemieux J.M., Molson J., Beaudoin G., Hébert R., 2016. Field evidence of CO<sub>2</sub> sequestration by mineral carbonation in ultramafic milling wastes, Thetford Mines, Canada. *International Journal of Greenhouse Gas Control* 47, 110-121.
- Liu C., Liu T., Wang D., 2018. Non-isothermal kinetics study on the thermal decomposition of brucite by thermogravimetry. *Journal of Thermal Analysis and Calorimetry* 134, 2339-2347.
- Mackenzie R.C., 1970. *Differential thermal analyses*. Academic Press, London, UK.
- Manuella F., 2011. Vein mineral assemblage in partially serpentinized peridotite xenoliths from Hyblean Plateau (south-eastern Sicily, Italy). *Periodico di Mineralogia* 80, 247-266.
- Newman T.E. and Hoffman G.K., 1996. Brucite Deposits in Marbke Canyon, Culberson County Texas. In: *Proceedings 31st Forum on the Geology of Industrial Minerals - The Borderland forum*. New Mexico Bureau of Mines Mineral Resources Bulletin 154, 37-42.
- Øvereng O., 2000. Granåsen, a dolomite/brucite deposit with potential for industrial development. *Norges Geologiske Undersøkelse, Bulletin* 436, 75-84.
- Pollastri S., Perchiazzi N., Lezzerini M., Plaisier J.R., Cavallo A., Dalconi M.C., Bursi Gandolfi N., Gualtieri A.F., 2016. The crystal structure of mineral fibres. 1. Chrysotile. *Periodico di Mineralogia* 85, 249-259.
- Pott F., Huth F., Friedrichs K.H., 1974. Tumorigenic effect of fibrous dusts in experimental animals. *Environmental Health Perspectives* 9, 313-315.
- Rausis K., Ćwik A., Casanova I., 2020. Phase evolution during accelerated CO<sub>2</sub> mineralization of brucite under concentrated CO<sub>2</sub> and simulated flue gas conditions. *Journal of CO<sub>2</sub> Utilization* 37, 122-133.
- Schilling J.H., 1968. The Gabbs Magnesite–Brucite Deposit, Nye County, Nevada. In: *Ore Deposits of the United States, 1933-1967: Graton-Sales*. (Ed.): J.D. Ridge, American Institute of Mining, Metallurgical and Petroleum Engineer, New York (USA), 1608-1621.
- Sheng Y., Jia H., Guo S., Taoum A., Guan B., Li H., Rui X., 2019. Effect of brucite fibers and early strength agent on cement stabilized macadam in Alpine regions. *International Journal of Pavement Research and Technology* 12, 315-324.
- Simandl G.J., Paradis S., Irvine M., 2007. Brucite - Industrial mineral with a future. *Geoscience Canada* 34, 57-64.
- Taufiq-Yap Y.H., Nur-Faizal A.R., Sivasangar S., Hussein M.Z., Aishah A., 2014. Modification of Malaysian dolomite using mechanochemical treatment via different media for oil palm fronds gasification. *International Journal Energy Research* 38, 1008-1015.
- Tran T.H., Steffen J.E., Clancy K.M., Bird T., Egilman D.S., 2019. Talc, Asbestos, and Epidemiology: Corporate Influence and Scientific Incognizance. *Epidemiology* 30, 783.
- Ward T.J., Spear T.M., Hart J.F., Webber J.S., Elashheb M.I., 2012. Amphibole asbestos in tree bark—a review of findings for this inhalational exposure source in Libby, Montana. *Journal of Occupational and Environmental Hygiene* 9, 387-397.
- WHO, 1997. Determination of airborne fibre number concentrations; a recommended method, by phase contrast optical microscopy (membrane filter method) <https://apps.who.int/iris/bitstream/handle/10665/41904/9241544961.pdf> (accessed 2021 Feb 10).
- Xiong R., Fang J., Xu A., Guan B., Liu Z., 2015. Laboratory investigation on the brucite fiber reinforced asphalt binder and asphalt concrete. *Construction and Building Materials* 83, 44-52.
- Yuanyi Y., Yi D., Xingkui L., 2019. Uniaxial compression mechanical properties and fracture characteristics of brucite fiber reinforced cement-based composites. *Composite Structures* 212, 148-158.
- Zoboli A., Di Giuseppe D., Baraldi C., Gamberini M.C., Malferrari D., Urso G., Lassinantti Gualtieri M., Bailey M., Gualtieri A.F., 2019. Characterisation of fibrous ferrierite in the rhyolitic tuffs at Lovelock, Nevada, USA. *Mineralogical Magazine* 83, 577-586.



This work is licensed under a Creative Commons Attribution 4.0 International License CC BY. To view a copy of this license, visit <http://creativecommons.org/licenses/by/4.0/>